PHYSICAL REVIEW A **93**, 063421 (2016)

Laser-subcycle control of sequential double-ionization dynamics of helium

Markus S. Schöffler,[1,*] Xinhua Xie (谢新华),[1] Philipp Wustelt,[2,3] Max Möller,[2,3] Stefan Roither,[1] Daniil Kartashov,[1] A. Max Sayler,[2,3] Andrius Baltuska,[1] Gerhard G. Paulus,[2,3] and Markus Kitzler[1,†]

[1]*Photonics Institute, Vienna University of Technology, 1040 Vienna, Austria*

[2]*Institute of Optics and Quantum Electronics, Friedrich Schiller University Jena, D-07743 Jena, Germany*

[3]*Helmholtz Institute Jena, D-07743 Jena, Germany*

(Received 26 February 2016; published 24 June 2016)

We present measured momentum distributions on the double ionization of helium with intense, near-circularly-polarized few-cycle laser pulses with a known carrier-envelope offset phase (CEP). The capability of obtaining CEP-resolved momentum distributions enables us to observe signatures of the various combinations of laser-half-cycle two-electron emissions. By comparison to semiclassical trajectory simulations, we succeed in assigning the corresponding structures in the measured distributions to certain two-electron emission dynamics. Based on this possibility, we demonstrate that the sequential double-ionization dynamics can be sensitively controlled with the pulse duration and the laser peak intensity. For the shortest pulse durations and not too high intensities we find that the two electrons are dominantly emitted with a delay of roughly a laser half cycle. For a just slightly increased intensity we find evidence that at least one of the two electrons is surprisingly likely emitted in between the peaks of the laser field oscillations rather than at the field maxima. The simulations reproduce the signatures of these kinds of two-electron emissions overall relatively well.

DOI: 10.1103/PhysRevA.93.063421

I. INTRODUCTION

Electron correlation is of fundamental importance in physics, chemistry, and biology. For example, it is central for the formation of molecular structure, acts as a driving force behind chemical reactions, determines the (dynamical) behavior of solid-state materials, and also plays an essential role in biological processes such as radiation damage or light harvesting. One of the most fundamental benchmark processes that is used in both experiments and theory for the investigation of dynamical electron-electron correlation effects is the removal of both electrons from the strongly correlated ground state of the helium atom. A variety of schemes such as charged-particle impact [1–6], single-photon absorption [7–10], and multiphoton processes [11–13] have been used to explore electron correlation in the initial and/or the final state during double ionization of helium.

The effects of electron correlation in double ionization are ultimately determined by the relative timing of the two ionization steps. This can be illustrated for helium by considering the process of ground-state relaxation after the first ionization step, i.e., the transformation from a screened helium atom with two indistinguishable electrons that both share the total binding energy of 79 eV equally (39.5 eV each), into an unscreened He^+ with a binding energy of 54.4 eV. In this process the relaxation of the wave function after the first ionization step leads to a fast loss of correlation between the two electrons. A well-known example for the loss of electron correlation due to this relaxation process is shake-off (SO) double ionization [14,15]. A fast removal of one electron due to, e.g., the absorption of an x-ray photon [8,10] or the capture of an electron during collision with a proton [5] causes a collapse of the wave function of the remaining electron. The projection of this wave function onto the new eigenstates shows that a small portion of the probability density is in the continuum, i.e., the probability for the emission of the second electron is nonzero. As time passes, the wave function relaxes and its overlap with the continuum and therewith the SO double-ionization rate gradually decreases. With increasing delay between the two ionization steps the correlation between the two electrons thus decays. To investigate this decay of electron correlation the two electrons need to be removed within the very short relaxation time of the ground state. This can be done by, e.g., impact ionization with relativistic highly charged ions or high-energy photons, where the double ionization can take place on subatomic units of time (<20 as). However, as these methods lack a timing reference, tracing the ionization dynamics with them is impossible and timing information can only be extracted indirectly by fitting a model to the measured spectra [2,5].

A timing reference in the attosecond domain is provided by the oscillations of strong laser fields [16]. Experiments on double ionization of helium with linearly polarized near-infrared strong laser fields in the intensity regime of nonsequential double ionization (NSDI) [17,18] have shown very distinct signatures of electron correlation [11,12]. In NSDI, similar to charged-particle collisional ionization [2,5], the double ionization is triggered by the field-driven impact of the first electron, which is strictly linked to the laser field oscillations and happens at certain well-defined instants within the laser cycle. Therefore, although in these experiments the laser field can serve as an attosecond timing reference, the delay between the two ionization events cannot be controlled externally. As a result, tracing the decay of correlation is again restricted to indirect methods.

Here we report on experiments that overcome this restriction by using close-to-circularly-polarized strong laser fields for which NSDI in helium is suppressed [19,20] and the two electrons are released by field ionization only. In this scheme, the relative timing between the two emission steps

*markus.schoeffler@tuwien.ac.at
†markus.kitzler@tuwien.ac.at

can be controlled by the duration and peak intensity of the laser pulse: While for long pulses the second electron can be emitted with a considerable delay [19], uninfluenced by the first ionization event, i.e., in an uncorrelated manner, we will show that for pulses with sub-two-cycle durations the emission dynamics of the two electrons is squeezed into laser-subcycle intervals. We obtain experimental access to this fast emission dynamics by applying the concept of angular streaking introduced by Maharjan *et al.* [21], now also known as the attoclock technique [22–26]. As we will show, attosecond timing information on the emission of the two electrons can be extracted from measured distributions of their sum momentum vector when it is referenced against the rotation of the laser polarization vector of the near-circularly-polarized laser pulses. This necessitates knowledge of the electric-field evolution of the laser pulses, which we obtained by measuring their carrier-envelope phase (CEP) in single-shot mode using a phase-meter device [27,28].

The capability of obtaining CEP-resolved momentum distributions enables us to observe the signatures of the various combinations of laser-half-cycle two-electron emissions. Guided by semiclassical simulations, we find that the various features in the measured CEP-resolved momentum distributions can in most cases be unambiguously assigned to a certain double-ionization dynamics with a specific delay between the two emission steps. Based on this possibility, we demonstrate that the sequential double-ionization dynamics can be sensitively controlled with the pulse duration and the laser peak intensity and that the delay between the two-electron emission steps can be tuned. For the shortest pulse durations (1.8 laser cycles) and not too high intensities ($\approx 6 \times 10^{15}$ W/cm^2) we find that the two electrons are dominantly emitted with a laser-subcycle delay between the two emission steps. For a just slightly increased intensity we find evidence that at least one of the two electrons is surprisingly likely emitted in between the peaks of the laser field oscillations rather than at the field maxima. The reason for this is yet to be identified. The signatures corresponding to these two effects are somewhat underestimated by a semiclassical model [29] that has recently been shown to yield good agreement with experimental data on the multiple ionization of neon by elliptically polarized multicycle laser pulses.

II. EXPERIMENTS

In our experiments we have used the cold target recoil ion momentum spectroscopy (COLTRIMS) technique [30,31] to measure the momentum vectors of ions originating from the interaction of intense laser pulses with helium atoms. The laser pulses in our experiments had durations ranging from 4.5 to 10 fs [full width at half maximum (FWHM) of intensity] and were generated by spectral broadening of 25-fs laser pulses from a home-built Ti:sapphire laser amplifier system (5-kHz repetition rate) in a gas capillary filled with several atmospheres of neon and subsequent temporal recompression with chirped mirrors and a pair of fused silica wedges. The wedge pair was also used to positively or negatively stretch the pulses up to 10 fs by increasing or decreasing the amount of glass in the beam path. The center wavelength of the pulses was 750 nm.

The laser beam was focused in an ultrahigh vacuum (UHV) chamber (base pressure 10^{-10} mbar) onto a supersonic gas jet of helium (precooled to 140 K) using a spherical silver mirror ($f = 60$ mm). Along the propagation direction of the laser beam (coordinate y) the gas jet (propagating along x) was cut by adjustable razor blades to about 20 μm, much shorter than the Rayleigh length of the laser beam ($\approx$200 μm). By this and by placing the focus of the laser beam slightly before the narrow jet smearing of the CEP due to the Gouy phase shift was avoided. Ionic fragments resulting from the interaction of the laser pulses with the helium jet were accelerated over 45 cm (along z) by a weak electric field (10 V/cm) onto a multihit capable time- and position-sensitive detector. The three-dimensional momenta of the ions were calculated from their impact positions on the detector and their time of flight, which for He^{2+} was about 4.3 μs.

The laser peak intensity was calibrated with an estimated precision of 15% to the laser power using the ion momentum distributions of He^+ measured well below the saturation intensity [32,33]. The laser peak intensity was adjusted via the such determined linear dependence on the laser power using pellicle beam splitters in transmission to reflect off an adjustable amount of laser power. A near-circular polarization state of the laser pulses was obtained using an ultrabroadband waveplate (Bernhard Halle Nachfolger GmbH). Despite the large bandwidth of our pulses, we reached circularities up to 95%, defined as the ratio of the electric-field strength perpendicular and parallel to the main axis of the polarization ellipse $E_\perp/E_\parallel$. This ratio and the direction of the axes of the polarization ellipse were measured outside the vacuum chamber using a broadband polarizer and *in situ* using ion momentum distributions in the laser polarization plane for laser intensities well below the He^+ saturation intensity. Both methods gave good agreement.

The experiments were performed in the so-called CEP-tagging mode [34,35], in which the laser pulse is split into two portions. A small portion is directed into a phase-meter device working with xenon gas [27,28] and the bigger portion is used in the COLTRIMS apparatus. From the asymmetry of above-threshold ionization (ATI) electron spectra measured along two opposite directions the CEP of the pulse [27,28] and its duration [36] were determined and monitored for each and every laser shot. In this scheme, the CEP value of the pulse in the phase meter is offset from the one in the COLTRIMS UHV chamber by a constant value. Calibration of this offset was performed by comparison to simulations, as described below. Further technical details can be found in [35,37–39].

III. ANGULAR MAPPING OF SEQUENTIAL DOUBLE IONIZATION

Measured momentum distributions of He^{2+} (integrated over all CEP values) in the laser polarization plane xz are shown in Figs. 1(a)–1(d) for four different pulse durations (FWHM) in between 4.5 and 10 fs and a constant peak intensity of 7×10^{15} W/cm^2. Removing both electrons from helium with (near-)circularly-polarized laser pulses necessitates a considerable peak intensity. Due to this necessity, the benchmark system of helium is a challenging choice for experimentally investigating the process of sequential double ionization (SDI).

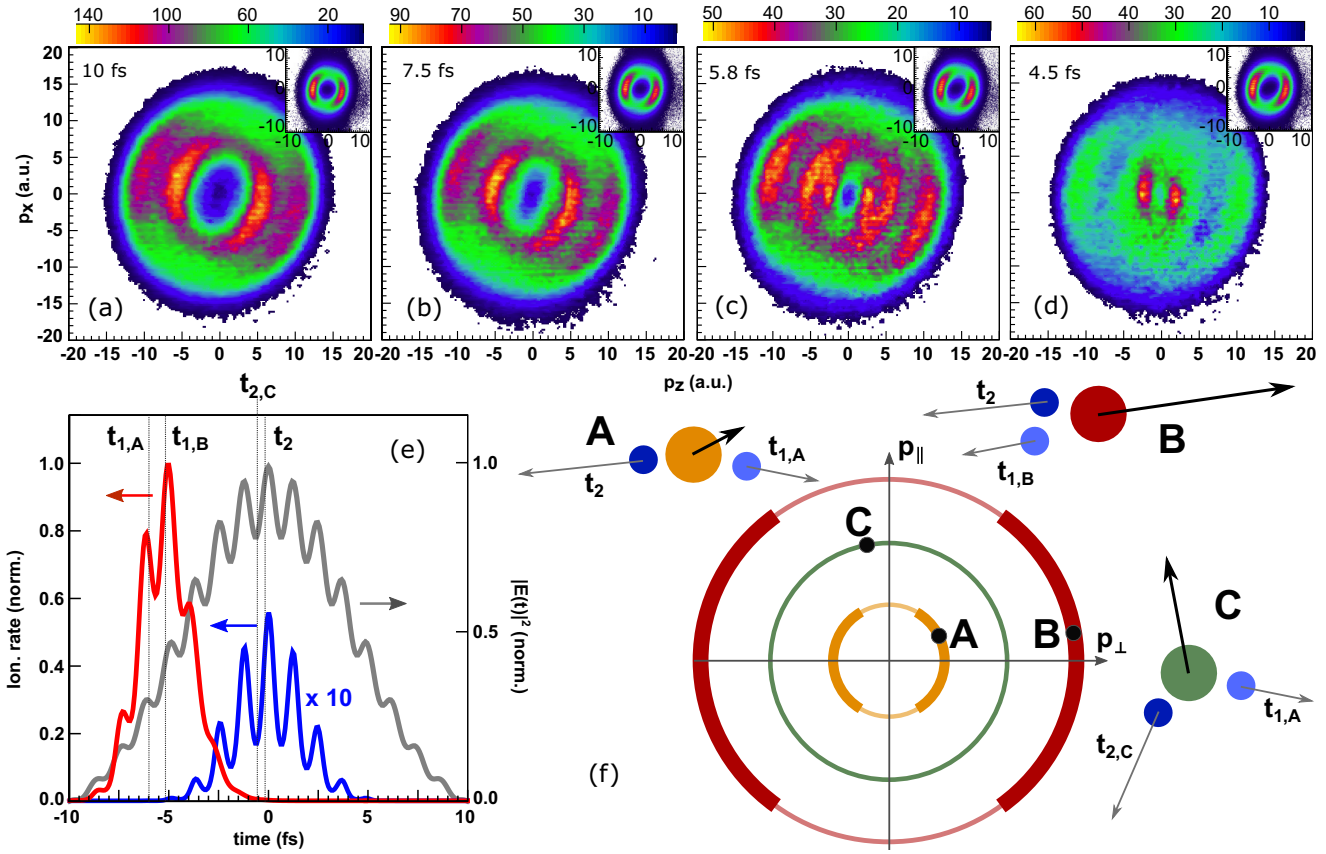

FIG. 1. (a)–(d) Measured He^{2+} momentum distributions in the polarization plane of near-circularly-polarized laser pulses (ellipticity $E_\perp/E_\parallel = 0.95$) with a peak intensity of 7×10^{15} W/cm^2 and a FWHM pulse duration of (a) 10 fs, (b) 7.5 fs, (c) 5.8 fs, and (d) 4.5 fs. The distributions have been integrated over all values of the CEP and over the third momentum coordinate. The insets show the corresponding He^+ momentum distributions. (e) Plot of $|E(t)|^2$ of the pulse from (a) with a CEP of 0 but with an ellipticity of 0.9 to enhance the visibility of the laser field oscillations (gray line). The corresponding ionization rates of the first and second emission steps as given by tunneling theory [40] are shown by red and blue lines, respectively. (f) Visualization of how the vectorial sum momentum of the two emitted electrons leads to the formation of the different structures in the measured spectra (rings and segments). The small and large closed circles represent electrons and ions, respectively. Three situations, denoted by A, B, and C, are shown. Black and gray arrows denote the momentum vectors of the ions and electrons, respectively. See the text for details.

Owing to the high peak intensity, we detected background originating from H_2^+, which has the same mass over charge ratio as He^{2+}. For the highest peak intensities the background rate was about 500 Hz out of 3000 Hz in total. The background was measured separately and subtracted from the final data. In the momentum distributions for He^{2+} the background is located around $p_x = 0$ a.u. and $p_z = -2.5$ a.u. with a Gaussian shape of width 11 a.u. (FWHM).

Figures 1(a)–1(d) show that, in contrast to the saturated momentum distributions of singly ionized helium (insets), the He^{2+} momentum distributions drastically change with pulse duration. The distributions measured with the two longest pulses, stretched to 10 and 7.5 fs, respectively, look relatively similar and qualitatively resemble those obtained previously for argon and neon with pulses around 30 and 7 fs, the shortest duration used so far in such experiments [21,24,25,29]. We have checked by simulations (described below) that the overall shape of the CEP-integrated distributions is similar for bandwidth-limited and chirped pulses within the parameter range used in the experiments. However, such chirp can influence the relative intensities of fine structures contained in the distributions [41] (see the discussion below). The origin of the double-segment ring structure contained in the momentum distributions in Figs. 1(a) and 1(b) is well understood and is due to the different possible combinations of the vectorial sum momentum of the two sequentially emitted electrons [21,24,42]. Depending on their emission times t_i, the two electrons ($i = 1,2$) may be emitted into different directions and gain different momenta in the laser field. Neglecting the influence of the ion's Coulomb potential, the electrons' momenta gained in the laser field are given by the laser vector potential at their release times, i.e., $\vec{p}_i^{\,e} = -\vec{A}(t_i)$, where $\vec{A}(t) = -\int_{-\infty}^{t} \vec{E}(t')dt'$, with $\vec{E}(t)$ the laser electric field. Thus, the structures in the He^{2+} momentum distribution reflect the distributions of the release times of the two electrons.

Figures 1(e) and 1(f) visualize this explanation for a 10-fs pulse. The absolute value of the laser electric field $|\vec{E}(t)|$ exhibits small oscillations that are due to the unavoidable imperfect circular polarization state of broadband laser pulses and that peak along the main axis of the polarization ellipse.

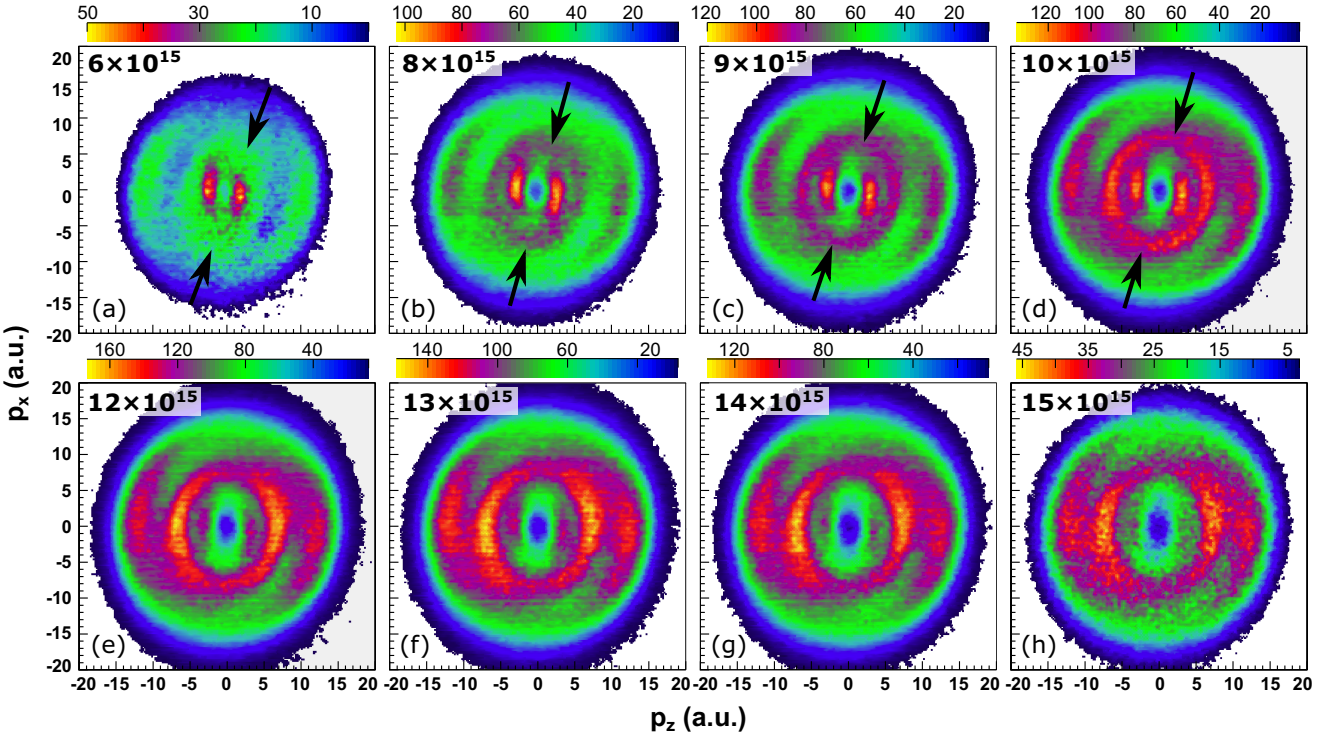

FIG. 2. Measured He^{2+} momentum distributions in the polarization plane of near-circularly-polarized laser pulses (ellipticity $E_\perp/E_\parallel = 0.95$) with a constant FWHM pulse duration of 4.5 fs and a peak intensity of (in units of 10^{15} W/cm^2) (a) 6, (b) 8, (c) 9, (d) 10, (e) 12, (f) 13, (g) 14, and (h) 15. The distributions have been integrated over all values of the CEP and over the third momentum coordinate. The black arrows mark a ring structure; see the discussion in the text.

Because of the strong nonlinear dependence of the ionization rate on the field strength [40,43,44] [blue and red curves in Fig. 1(e)], the two electrons are dominantly emitted along the main axis of the polarization ellipse ($\parallel$) every laser half cycle and their final momenta point perpendicular to this axis ($\perp$) [45]. Depending on whether the delay between the first and second emission is an even or odd number of half cycles, the two electrons are emitted either into the same or into opposite directions [cf. the sketch in Fig. 1(f)]. As due to momentum conservation, the He^{2+} ion momentum is the negative sum of the two electron momenta $\vec{p}_{He^{2+}} = -(\vec{p}^{\,e}_1 + \vec{p}^{\,e}_2)$; this results in either a large (for emission into the same direction) or a smaller sum momentum (for emission into opposite directions), which is the reason for the appearance of the two ring segments in the measured distributions in Figs. 1(a) and 1(b). Two situations that lead to a sum momentum within two different ring segments, marked by A and B, are shown in Fig. 1(f). The situation marked by C leads to a sum momentum pointing into a direction almost perpendicular to those of situations A and B. Such a sum momentum has not been observed in experiments so far. We will return to this situation below.

Sub-cycle ionization structures

As the ionization rate exhibits a peak every laser half cycle [cf. Fig. 1(e)], for multicycle pulses electron emission may take place over many laser cycles. Thus, even though in intense laser pulses the first emission step due to ionization saturation may happen within only a short time window on the rising edge of the laser pulse and therewith the momentum of the first electron is fixed to roughly 5 a.u. [see the insets of Figs. 1(a)–1(d)], the multicycle emission structure of the second electron that is emitted at higher field strengths should actually give rise to several ring segments [42]. However, as for long pulses the pulse envelope and therefore $\vec{p}^{\,e}_2 = -\vec{A}(t_2)$ changes relatively little from cycle to cycle and these structures are additionally washed out by focus volume averaging, it is difficult to observe them in experiments and only two segments are dominantly observed [21,24,25,29].

If the pulse duration is reduced to the few-cycle regime, though, the difference in $\vec{p}^{\,e}_2 = -\vec{A}(t_2)$ between different half cycles becomes larger and the sub-cycle emission structures should become observable. Indeed, for a pulse duration of 5.8 fs a third pair of segments at small momenta becomes visible in the He^{2+} momentum distribution [Fig. 1(c)]. Now, if the pulse duration is further decreased by merely $\sim$1 fs to 4.5 fs, the ion momentum distribution changes dramatically and this third segment at small ion momenta becomes the dominant structure.

To understand this dramatic change at the short-pulse limit, we measured the He^{2+} momentum distributions for various laser peak intensities from 6×10^{15} to 1.5×10^{16} W/cm^2 for a constant pulse duration of 4.5 fs (see Fig. 2). As can be seen, already for an intensity slightly higher than the one used in Fig. 1 [8×10^{15} W/cm^2, Fig. 2(b)], a nearly homogeneous ring becomes visible in between the low-momentum structure of Fig. 2(a) and the high-momentum ring segment of Figs. 1(a)–1(c). With further increasing intensity the innermost peaks (almost) vanish and the central ring fades into the ring

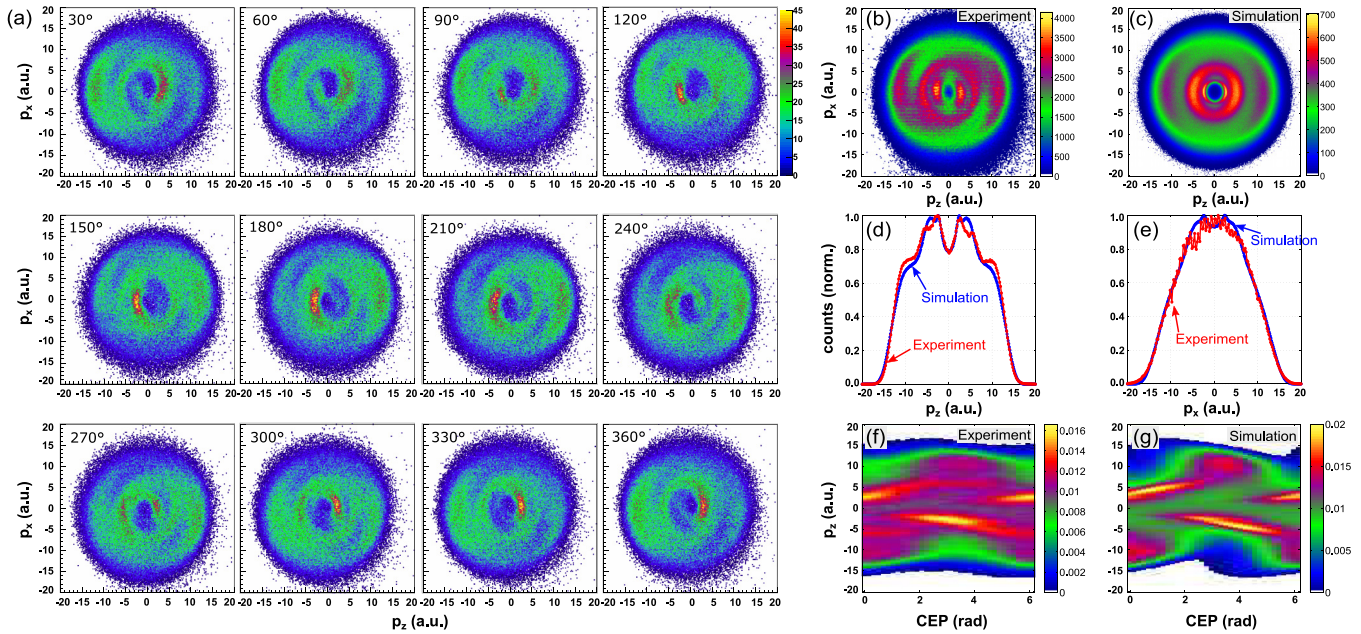

FIG. 3. (a) Measured He^{2+} momentum distributions in the polarization plane of near-circularly-polarized laser pulses (ellipticity $E_\perp/E_\parallel = 0.95$) with a constant FWHM pulse duration of 4.5 fs and a peak intensity of 10×10^{15} W/cm^2 for different values of the CEP (as indicated in the panels). (b) Momentum distribution resulting when the distributions from (a) are integrated over all values of the CEP [which results in the distribution in Fig. 2(d), here reproduced for reference purposes]. (c) Corresponding momentum distribution simulated by the CTMC method (see the text for details). (d) and (e) Measured and simulated momentum distributions from (b) and (c), respectively, along the (d) p_z and (e) p_x directions, with the other directions integrated over. (f) and (g) The CEP dependence of the (f) measured and (g) simulated momentum distributions along p_z (with all other directions integrated over).

segments of Figs. 1(a) and 1(b). The feature thus only appears for very short pulses and only in a certain intensity regime. In order to understand its origin one needs to obtain insight into the two-electron emission dynamics taking place on a laser-subcycle time scale, as we will show in the following.

IV. SUB-CYCLE MAPPING OF TWO-ELECTRON EMISSION DYNAMICS

Sub-cycle and even sub-half-cycle temporal resolution is obtained if the different contributions to the He^{2+} momentum distribution from the separate half-cycle ionization bursts can be disentangled. As we will show, the separate bursts and their attosecond evolution can be clearly identified in the CEP-resolved He^{2+} momentum distributions, exemplarily shown in Fig. 3(a) for the strongly structured He^{2+} momentum distribution from Fig. 2(d), which for reference is reproduced also in Fig. 3(b). Figures 3(d) and 3(e) show the CEP-integrated momentum distribution along p_z and p_x, respectively, in comparison with simulations (see the discussion below). Animated versions of the CEP-resolved momentum distributions in Fig. 3(a) and of the corresponding ones for He^+ are provided in the Supplemental Material [46]. It can be seen that the He^{2+} momentum distributions for a given CEP consist of two spirals, one coiling counterclockwise from the center outward and the other one coiling clockwise. The changes of the momentum distribution along p_z with the CEP are plotted in Fig. 3(f). This figure clearly shows the alternation of the two-electron emission along p_z with the CEP. The asymmetry of two-electron emission due to the asymmetric field shape of the short laser pulses is thus unambiguously mapped into the momentum distributions. The spirals in Fig. 3 hence reflect the rotating evolution of the laser field vector in the polarization plane, which for a center wavelength of 750 nm rotates over 2π within 2.5 fs. The rotation of the field vector thus establishes an attosecond timing reference in the angular direction [21]. It is this timing reference that we will now exploit to find the emission times t_1 and t_2 of the first and second electrons from the measured He^{2+} momentum distributions in Fig. 3(a).

To understand the origin of each of the structures (peaks and segments) in Fig. 3, we will now compare the measured momentum distributions to those obtained from simulations using the classical-trajectory Monte Carlo (CTMC) method. Recently, it was shown that this method gives good agreement for the CEP-integrated multiple ionization of neon with 35-fs-long elliptically polarized laser pulses [29]. Details on the method and its implementation can be found in Ref. [29]. In short, the simulations assume a strictly sequential double-ionization dynamics with no interaction between the two emitted electrons. Likewise, the influence of the ion's Coulomb potential on the emitted electrons is neglected. Both electron release events are assumed to take place strictly by tunneling with a rate given by tunnel ionization models [43,44]. Barrier suppression is taken into account empirically as described in Ref. [40]. Ionization saturation and laser focus intensity averaging are fully accounted for by assuming a beam geometry with the same parameters as in the experiments. Momentum distributions obtained by the CTMC simulations are shown in Figs. 3 and 4 in direct comparison with measured distributions.

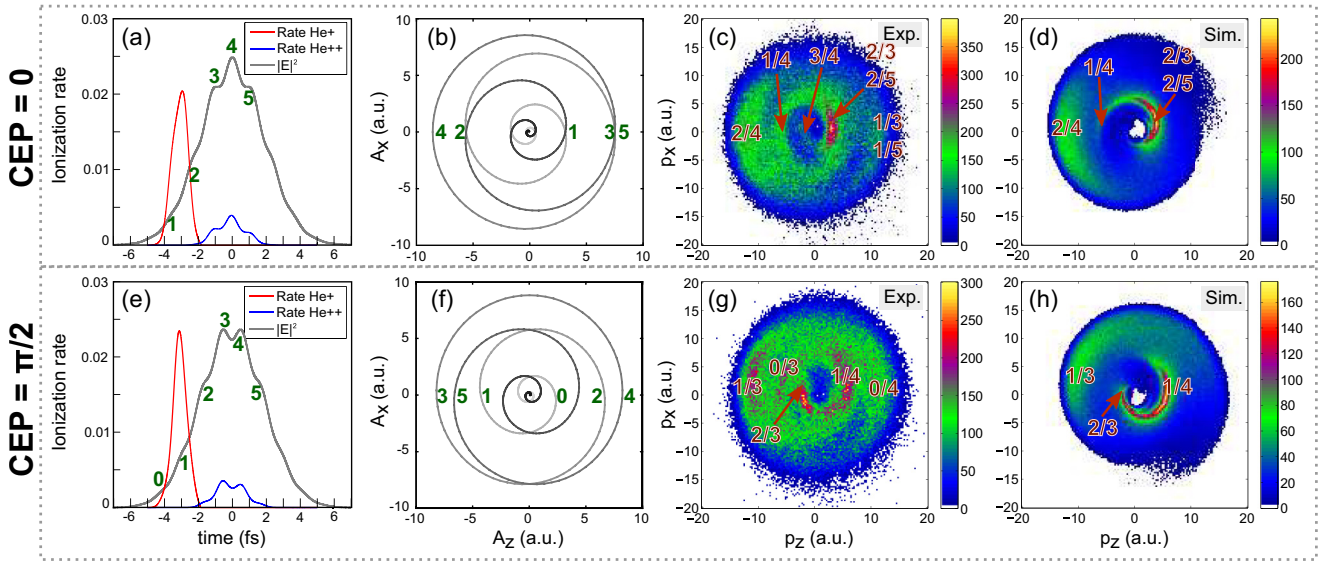

FIG. 4. (a) Intensity profile $|E(t)|^2$ of a pulse with a duration of 4.5 fs, an ellipticity $E_\perp/E_\parallel = 0.95$, and a peak intensity of 10×10^{15} W/cm^2 for a CEP of 0 (gray line) together with the corresponding ionization rates of the first (red line) and second (blue line) emission steps as given by tunneling theory [40]. (b) Evolution of the vector potential $\vec{A}(t)$ in the polarization plane of the pulse in (a). (c) Measured He^{2+} momentum distribution for the pulse given in (a). (d) Corresponding momentum distribution simulated by the CTMC method. (e)–(h) Same as (a)–(d) but for a pulse with a CEP of $\pi/2$. The numbers in the momentum distributions correspond to the numbered half cycles in (a) and (b) and in (e) and (f).

Assignment of ionization bursts

Using the momentum distributions obtained with the CTMC model, the segments and peaks in the He^{2+} momentum distributions in Fig. 3 can be assigned to a certain two-electron emission dynamics. This is demonstrated in Fig. 4 for the two momentum distributions from Fig. 3 with CEP values 0 [Figs. 4(a)–4(d)] and $\pi/2$ [Figs. 4(e)–4(h)]. Figures 4(a) and 4(e) show $|E(t)|^2$ (gray) and the ionization rates for the emission of the first (red) and second (blue) electrons, respectively. While due to ionization saturation the first electron release takes place during less than one optical cycle at the rising edge of the pulse, the second, more strongly bound electron is mainly released around the pulse maximum. Thus, all ionization dynamics takes place within less than two optical cycles. The evolution of the vector potential in the laser polarization plane, where time increases from light to dark, is shown in Figs. 4(b) and 4(f). Figures 4(c), 4(d), 4(g), and 4(h) show the measured He^{2+} momentum distributions in comparison with the corresponding simulated ones obtained using the CTMC model. For this comparison the constant CEP offset value, which arises in our experimental scheme and is mentioned above, could be easily calibrated without ambiguity because of the many peaks and segments in the He^{2+} momentum distributions. Once the CEP offset was calibrated, it was kept for all simulations.

The measured and simulated distributions agree very well in the main structures, but there are subtle differences between them. We will discuss these differences below. First, we will describe how each peak in the momentum distributions can be assigned to a specific two-electron emission dynamics. To see this, we label each half cycle of the electric-field oscillations and the corresponding ionization bursts with a number. Then, by using the relation $\vec{p}_{He^{2+}} = -[\vec{p}^{\,e}_1(t_1) + \vec{p}^{\,e}_2(t_2)]$ visualized in Fig. 1 we can identify each possible combination of ionization bursts for the first and second electrons in the measured and simulated momentum distributions. Because ionization of the first electron quickly saturates and emission of the second electron is confined to a narrow time window around the peak of the laser pulse, the possible combinations of half cycles that can lead to a certain segment in the momentum distributions is very limited and thus this assignment can in most cases be done unambiguously. The peaks in the momentum distributions correspond to combinations when both ionization rates of the first and second electrons show a (relative) maximum. The extended spiral-shaped segments reflect two-electron emission taking place over more than one half cycle.

To exemplify the assignment of the ionization bursts let us discuss three specific cases. The first example is the segment on the left side of the momentum distributions (around $p_z = -12$ a.u.) for a CEP of zero. This segment is caused when the first electron is released during half cycle 2 and the second electron exactly one optical cycle later (half cycle 4). For both half cycles the vector of the laser vector potential points in the negative p_z direction. Thus, $\vec{p}^{\,e}_1 = -\vec{A}(t_1)$ and $\vec{p}^{\,e}_2 = -\vec{A}(t_2)$ add up to the large negative recoil momentum along p_z for the He^{2+} ion. The second example is the two strong peaks in the center for a CEP of $\pi/2$ at $p_z \approx -2$ a.u. and $p_z \approx 6$ a.u. These correspond to the strongest peaks 3 and 4 in the ionization of the second electron. Because the He^{2+} momentum is small, the momentum vectors of the first and second electrons must point in approximately opposite directions such that their sum momentum is a small value. Therefore, these peaks can be unambiguously identified as two-electron emission during the half cycles 2 and 3 (for $p_z \approx -2$ a.u.) and half cycles 1 and 4

(for $p_z \approx 6$ a.u.). As a last example we discuss a segment that cannot be assigned unambiguously, namely, the one around $p_z \approx 3$ a.u. for a CEP of zero. This strong segment can be due to two-electron emission during half cycles 2 and 3 or during 2 and 5, respectively. The reason for the ambiguity is that for a CEP of zero the laser electric field is symmetric about the pulse peak. Therefore, contributions from half cycles 3 and 5 cannot be distinguished.

V. DISCUSSION OF THE TWO-ELECTRON EMISSION DYNAMICS

The assignment of the structures in the CEP-resolved He^{2+} momentum distributions to a certain sequential double-ionization dynamics demonstrated in Fig. 4 reveals a clear trend for the relative timing of the two-electron emission events: Double-ionization events for which the two electrons are emitted with a delay of around one or two laser cycles T or $2T$ lead to the largest $p_r = \sqrt{\vec{p}_x^{\,2} + \vec{p}_z^{\,2}}$ visible in the measured He^{2+} momentum distributions in Fig. 2. Still larger p_r would result from two-electron emissions that take place within the same half cycle with a near-zero delay (cf. Fig. 1). We can therefore conclude that in our experiments we do not observe such double-ionization dynamics. If the two electrons are emitted with a delay of one half cycle $T/2$, they give rise to segments with small p_r. Two-electron emission events for which the delay is $1.5T$ finally lead to intermediate p_r values, in between those corresponding to T and $T/2$. In the following we will discuss two interesting cases of double-ionization dynamics that are revealed by our experiments.

A. Laser-subcycle two-electron emission

From the viewpoint of electron correlation effects, very interesting double-ionization dynamics are those where the two electrons are emitted with a small delay below one laser period T. As explained above, delays around $T/2$ lead to structures with small p_r values. Peaks and segments with a small $p_r \approx 3$ a.u. can be seen in Fig. 3 for all CEP values, but the intensity and positions of these structures vary with the CEP. These variations of the low-energy peak are particularly pronounced along the p_z direction as shown in Fig. 3(f). The events forming this peak at small p_r raise important questions: Do they carry information on the decay of the ground state initiated by the first ionization step, as sketched in the Introduction? Are these electron pairs correlated with each other and, if so, to what degree?

A comparison of the measured distributions with those simulated by the CTMC method [cf. Figs. 3(b)–3(g)] shows that the segments with the small $p_r \approx 3$ a.u. are narrower and weaker in the simulated distributions. This is interesting, since most of the other structures are quite satisfactorily reproduced by the simulations. Furthermore, for neon the same CTMC model could successfully reproduce the measured CEP-integrated momentum distributions in the multicycle regime with high precision [29]. Thus, it seems that either the case of helium or the very short pulse duration used here causes the model to partially break down. One of the reasons for this can be the neglected correlation between the two electrons [42].

However, there are a number of other possibilities that can lead to a discrepancy between the measured and simulated momentum distributions, such as the neglect of the influence of the ion's Coulomb potential or subtle differences between the laser fields used in the experiment and those assumed in the simulations. Such differences could be, for example, a (small) residual chirp or a different pulse shape. In particular, in our experiments we cannot exclude the existence of a (weak) prepulse, which is easily generated during spectral broadening of our pulses by nonlinear pulse propagation in the hollow core fiber filled with neon gas. Such a prepulse would not be noticed in our experiments as we estimate the duration of our pulses from the asymmetry of the ATI electron spectra measured with the phase meter (see Sec. II). These spectra are insensitive to a weak prepulse as long as the highest electron energies beyond the $2U_p$ cutoff, with U_p the ponderomotive potential [47], are generated by the stronger main pulse.

To investigate whether the discrepancy could be caused by a prepulse, we performed a series of simulations with laser pulses that exhibit different third-order variations of the spectral phase. Additionally, we also varied the second-order phase, the peak intensity, and the bandwidth-limited duration of the laser pulses. While the overall shapes of the momentum distributions do not critically depend on variations of these quantities within reasonable ranges around the values used in the measurements, we find that the relative intensities of certain peaks can vary notably with the pulse parameters, in particular in the CEP-resolved distributions. The segments at small $p_r \approx 3$ a.u. that correspond to laser-subcycle two-electron emission events and are considerably narrower and weaker in the CEP-integrated simulated distributions in Fig. 3 are enhanced in the latter distributions if a slightly shorter bandwidth-limited pulse duration is assumed. Furthermore, already for small second-order chirp the inner ring becomes weaker. Thus, the pulses used in the experiment might have been even slightly shorter than 4.5 fs and were essentially at their bandwidth-limited duration. In contrast, the assumption of the presence of a third-order phase variation and therewith a prepulse can, for certain values of the CEP, enhance these peaks in the CEP-resolved distributions shown in Fig. 4. Yet the agreement between measured and simulated CEP-integrated momentum distributions (Fig. 3) becomes worse if third-order chirp is assumed in the simulations. A detailed account of these extensive simulations is, however, well beyond the scope of the current paper and will be given elsewhere [41]. Also, it will be interesting to further investigate the reasons for the appearance of the strong laser-subcycle double-ionization features revealed by our experiments by more elaborate numerical models than the CTMC method.

Important insight into the two-electron emission dynamics underlying the features with small p_r can be drawn based on the experimentally obtained dependence of the He^{2+} momentum distributions on the laser pulse parameters. It can be seen in Figs. 1 and 2 that laser-subcycle double-ionization events are strongly (relatively) enhanced for the shortest pulse duration (cf. Fig. 1) and for small, rather than large, peak intensity (cf. Fig. 2). Both observations can be intuitively understood: For long pulses ionization can proceed over several laser half cycles. However, as the pulse duration gets shorter, the half cycles with the highest ionization rate will

move closer to the laser pulse peak. Thus, also the delay between the two ionization bursts during which the two electrons are emitted will get smaller, until at a very short pulse duration the two electrons are both emitted during a single laser cycle only. The two ionization events will thus be squeezed in time by the short laser pulse envelope.

High pulse intensity, however, counteracts this squeezing mechanism, as the first ionization event becomes saturated already at the rising edge of the laser pulse. The first electron is thus emitted the earlier the higher the peak intensity is. As long as the intensity is low enough such that the ionization of the second electron is not saturated, the second electron emission will always take place around the pulse peak. Thus, for a given pulse duration the delay between the two emissions increases with peak intensity. For small intensity and short pulse duration, on the other hand, saturation of the first ionization step is suppressed until shortly before or until the pulse peak. Therefore, for relatively small laser intensities the ionization rates of the first and second electrons show a significant overlap and emission during a single laser cycle is likely. This can be clearly seen in Fig. 2 by the relative increase of the segments with $p_r \approx 3$ a.u. for decreasing peak intensity, which shows a maximum for the smallest intensity in Fig. 2(a). Naturally, the absolute value of the double-ionization probability decreases with decreasing peak intensity (cf. the different intensity scales in Fig. 2). Our experiments thus show that the relative timing in sequential double ionization can be controlled by pulse duration and intensity. Future experiments and simulations aimed at investigating the correlation of the two electrons should thus study the sequential double-ionization process for low intensity and very short pulse durations.

B. Laser-asynchronous two-electron emissions

The second interesting feature in the He^{2+} momentum distributions that we would like to discuss is the closed-ring structure at intermediate $p_r \approx 7$ a.u. values that appears for not too high intensities [Figs. 2(a)–2(d), marked by arrows in the figures] and a very short pulse duration. This closed-ring structure is weak for small intensities [cf. Fig. 2(a)] and gradually opens up and turns into ring segments with identical p_r for both high peak intensity [cf. Figs. 2(e)–2(h)] and longer pulse duration [cf. Figs. 1(a)–1(c)]. Figure 3(a) shows how the closed-ring structure is formed in the CEP-integrated distributions: Contributions to the ring structure are clearly visible as parts of a spiral at $p_r \approx 7$ a.u. for almost all CEP values. These spirals add up to the closed-ring structure in the CEP-integrated momentum distribution shown in Fig. 3(b).

The uniform angular intensity distribution of the ring structure is distinctively different from that of those structures that are due to double-ionization events with delays $T/2$ ($p_r \approx 3$ a.u.) and $1T/2T$ ($p_r \approx 12$ a.u.). The ionization events forming those structures take place strictly synchronized with the laser field oscillations at its peaks and are thus emitted when the laser field vector points along the main axis of the polarization ellipse, which results in segments rather than rings. Likewise, those parts of the closed-ring structures that are situated in between the peaks at $p_r \approx 3$ a.u. and $p_r \approx 12$ a.u. along the main axis of the polarization ellipse are also caused by ionization events taking place at the peaks of the laser field oscillations with delays around $1.5T$ [see Figs. 4(c) and 4(d)]. Thus, the double-ionization events causing those parts of the ring structures marked by arrows in Fig. 2 obviously exhibit a different sensitivity on the ellipticity of the laser field than the strictly synchronized emission events. To obtain a ring structure, the sum momentum of the two electrons $\vec{p}_{He^{2+}} = -[\vec{p}^{\,e}_1(t_1) + \vec{p}^{\,e}_2(t_2)]$ must point in a direction roughly orthogonal to that of all other structures. One possibility for this could be pronounced Coulomb effects between the electrons and the ion and/or among the two electrons such that an almost 90° rotation of the emission directions of the two electrons is caused. Another possibility is that the two electrons are emitted at instants that are not strictly separated by exactly two or three laser half cycles but rather by odd values in the range of approximately $0.7T$–$1.8T$ (e.g., $1.3T$, but not too close to $1T$ and $1.5T$). This also leads to a rotated sum momentum direction of the two electrons, as visualized by situation *C* in Fig. 1(f). Thus, the double-ionization events that form the ring structure might be caused by emissions in between the peaks of the laser oscillations, i.e., asynchronously to the laser field peaks.

Either way, strong Coulomb rotation or asynchronous emission, so far such two-electron emission has not been observed in experiments. One reason for this might be that so far all experiments that were investigating sequential double-ionization dynamics, e.g., Refs. [21,24–26,29,48], were performed with pulses that consisted of multiple laser cycles. However, our measurements show that the clear ring structure with an almost homogeneous angular intensity distribution can only be observed for very short sub-two-cycle pulses. This becomes clear by comparison of the momentum distributions measured for longer pulses (Fig. 1) with those obtained with the short pulses (Fig. 2). As mentioned above, from Fig. 2 it also becomes clear that the contributions of these events is most pronounced for not too high intensities. Thus, the emission dynamics underlying the closed-ring structures takes place most effectively for the same laser pulse parameters as the sub-cycle emissions discussed in the previous section.

A double-ionization dynamics where either the first or the second or both electrons are emitted in between the laser field peaks is in principal in full accord with conventional tunnel ionization caused by nearly circularly polarized laser pulses, as can be inferred from the significant ionization rate in between the peaks of the laser field [see blue lines in Figs. 4(a) and 4(e)]. For the high ellipticity achieved in our experiments electrons are thus released with high probability also in between the field maxima and thus can lead to ion momenta pointing into the direction perpendicular to the main emission axis, as visualized by situation *C* in Fig. 1(f). However, the CTMC simulations based on this evolution of the ionization rate slightly underestimate the closed-ring structures as compared to the experimental observation [compare, for example, Figs. 3(b) and 3(c)]. Either this is due to a process that is not incorporated in the CTMC model, such as the Coulomb interaction, or this is caused by a slight deviation of the experimental pulse parameters from the idealized ones assumed in the simulations. Further numerical investigations performed with the aim of understanding this slight discrepancy and the double-ionization dynamics leading to the closed-ring structure are left for future study [41].

VI. CONCLUSION

We have reported momentum-resolved data on the double ionization of helium with intense, close-to-circularly-polarized laser pulses. The momentum distributions of He^{2+} in the laser polarization plane obtained with sub-two-cycle laser pulses with a known carrier-envelope offset phase show rich structure and a strong dependence on the duration, peak intensity, and CEP of the pulses. By comparison with classical trajectory Monte Carlo simulations that have been shown to model multiple ionization of neon with multicycle-long elliptically polarized laser pulses very well [29], we are able to assign the experimentally observed CEP-resolved momentum structures to certain two-electron emission dynamics. Thus, we succeed in resolving the different contributions of the half-cycle ionization bursts [42] to the overall momentum distribution. This achievement, on the one hand, reveals two interesting cases of two-electron emission dynamics and, on the other hand, allows us to study in detail their dependence on pulse intensity and duration. The first interesting finding is that for the shortest laser pulses and for relatively low peak intensity the two electrons are emitted most probably with a mere delay of about one laser half cycle. The second notable finding is that for few-cycle pulses the two electrons may also be emitted very likely in between the peaks of the electric-field oscillations. Both features are, on a large scale, reproduced by the CTMC simulations. Deviations on a finer scale might be due to a neglect of Coulomb interactions and/or due to simplified assumptions regarding the laser pulse parameters in the simulations. Additional numerical investigations with more realistic pulse parameters are underway [41].

ACKNOWLEDGMENTS

We gratefully acknowledge discussions with X. M. Tong about details of the ionization rate. This work was funded by the Austrian Science Fund (FWF) under Grants No. P21463-N22, No. P28475-N27, No. P25615-N27, No. P27491-N27, and No. SFB-F49 NEXTlite; by a starting grant from the ERC (project CyFi); by the German Research Foundation (DFG) under Grant No. PA730/4 and under the DFG Priority Programme 1840; and by ECs Seventh Framework Programme (LASERLAB-EUROPE III, Grant No. 284464).

[1] T. N. Rescigno, Science **286**, 2474 (1999).
[2] T. Weber, K. Khayyat, R. Dörner, V. Mergel, O. Jagutzki, L. Schmidt, F. Afaneh, A. Gonzalez, C. L. Cocke, A. L. Landers, and H. Schmidt-Böcking, J. Phys. B **33**, 3331 (2000).
[3] A. Dorn, A. Kheifets, C. D. Schröter, B. Najjari, C. Höhr, R. Moshammer, and J. Ullrich, Phys. Rev. Lett. **86**, 3755 (2001).
[4] M. Schulz, R. Moshammer, D. Fischer, H. Kollmus, D. H. Madison, S. Jones, and J. Ullrich, Nature (London) **422**, 48 (2003).
[5] M. Schöffler, A. L. Godunov, C. T. Whelan, H. R. J. Walters, V. S. Schipakov, V. Mergel, R. Dörner, O. Jagutzki, L. P. H. Schmidt, J. Titze, E. Weigold, and H. Schmidt-Böcking, J. Phys. B **38**, L123 (2005).
[6] M. Dürr, A. Dorn, J. Ullrich, S. P. Cao, A. Czasch, A. S. Kheifets, J. R. Götz, and J. S. Briggs, Phys. Rev. Lett. **98**, 193201 (2007).
[7] J. S. Briggs and V. Schmidt, J. Phys. B **33**, R1 (2000).
[8] A. Knapp, A. Kheifets, I. Bray, T. Weber, A. L. Landers, S. Schössler, T. Jahnke, J. Nickles, S. Kammer, O. Jagutzki, L. P. H. Schmidt, T. Osipov, J. Rösch, M. H. Prior, H. Schmidt-Böcking, C. L. Cocke, and R. Dörner, Phys. Rev. Lett. **89**, 033004 (2002).
[9] I. Bray, D. Fursa, A. Kadyrov, A. Stelbovics, A. Kheifets, and A. Mukhamedzhanov, Phys. Rep. **520**, 135 (2012).
[10] M. S. Schöffler, C. Stuck, M. Waitz, F. Trinter, T. Jahnke, U. Lenz, M. Jones, A. Belkacem, A. L. Landers, M. S. Pindzola, C. L. Cocke, J. Colgan, A. Kheifets, I. Bray, H. Schmidt-Böcking, R. Dörner, and Th. Weber, Phys. Rev. Lett. **111**, 013003 (2013).
[11] A. Rudenko, V. L. B. de Jesus, Th. Ergler, K. Zrost, B. Feuerstein, C. Schröter, R. Moshammer, and J. Ullrich, Phys. Rev. Lett. **99**, 263003 (2007).
[12] A. Staudte, C. Ruiz, M. Schöffler, S. Schössler, D. Zeidler, Th. Weber, M. Meckel, D. M. Villeneuve, P. B. Corkum, A. Becker, and R. Dörner, Phys. Rev. Lett. **99**, 263002 (2007).
[13] M. Kurka *et al.*, New J. Phys. **12**, 073035 (2010).
[14] T. Åberg, Phys. Rev. **156**, 35 (1967).
[15] T. Y. Shi and C. D. Lin, Phys. Rev. Lett. **89**, 163202 (2002).
[16] F. Krausz and M. Ivanov, Rev. Mod. Phys. **81**, 163 (2009).
[17] D. N. Fittinghoff, P. R. Bolton, B. Chang, and K. C. Kulander, Phys. Rev. Lett. **69**, 2642 (1992).
[18] B. Walker, B. Sheehy, L. F. DiMauro, P. Agostini, K. J. Schafer, and K. C. Kulander, Phys. Rev. Lett. **73**, 1227 (1994).
[19] D. N. Fittinghoff, P. R. Bolton, B. Chang, and K. C. Kulander, Phys. Rev. A **49**, 2174 (1994).
[20] F. Mauger, C. Chandre, and T. Uzer, Phys. Rev. Lett. **105**, 083002 (2010).
[21] C. M. Maharjan, A. S. Alnaser, X. M. Tong, B. Ulrich, P. Ranitovic, S. Ghimire, Z. Chang, I. V. Litvinyuk, and C. L. Cocke, Phys. Rev. A **72**, 041403 (2005).
[22] P. Eckle, A. N. Pfeiffer, C. Cirelli, A. Staudte, R. Dörner, H. G. Muller, M. Büttiker, and U. Keller, Science **322**, 1525 (2008).
[23] P. Eckle, M. Smolarski, P. Schlup, J. Biegert, A. Staudte, M. Schöffler, H. G. Muller, R. Dörner, and U. Keller, Nat. Phys. **4**, 565 (2008).
[24] A. N. Pfeiffer, C. Cirelli, M. Smolarski, R. Dörner, and U. Keller, Nat. Phys. **7**, 428 (2011).
[25] A. N. Pfeiffer, C. Cirelli, M. Smolarski, X. Wang, J. H. Eberly, R. Dörner, and U. Keller, New J. Phys. **13**, 093008 (2011).
[26] A. N. Pfeiffer, C. Cirelli, M. Smolarski, and U. Keller, Chem. Phys. **414**, 84 (2013).
[27] A. M. Sayler, T. Rathje, W. Müller, K. Rühle, R. Kienberger, and G. G. Paulus, Opt. Lett. **36**, 1 (2011).
[28] T. Rathje, N. G. Johnson, M. Möller, F. Süßmann, D. Adolph, M. Kübel, R. Kienberger, M. F. Kling, G. G. Paulus, and A. M. Sayler, J. Phys. B **45**, 074003 (2012).
[29] P. Wustelt, M. Möller, T. Rathje, A. M. Sayler, T. Stöhlker, and G. G. Paulus, Phys. Rev. A **91**, 031401 (2015).
[30] J. Ullrich, R. Moshammer, R. Dörner, O. Jagutzki, V. Mergel, H. Schmidt-Böcking, and L. Spielberger, J. Phys. B **30**, 2917 (1997).

[31] R. Dörner, V. Mergel, O. Jagutzki, L. Spielberger, J. Ullrich, R. Moshammer, and H. Schmidt-Böcking, Phys. Rep. **330**, 95 (2000).
[32] A. S. Alnaser, X. M. Tong, T. Osipov, S. Voss, C. M. Maharjan, B. Shan, Z. Chang, and C. L. Cocke, Phys. Rev. A **70**, 023413 (2004).
[33] C. Smeenk, J. Z. Salvail, L. Arissian, P. B. Corkum, C. T. Hebeisen, and A. Staudte, Opt. Express **19**, 9336 (2011).
[34] N. G. Johnson, O. Herrwerth, A. Wirth, S. De, I. Ben-Itzhak, M. Lezius, B. Bergues, M. F. Kling, A. Senftleben, C. D. Schröter, R. Moshammer, J. Ullrich, K. J. Betsch, R. R. Jones, A. M. Sayler, T. Rathje, K. Rühle, W. Müller, and G. G. Paulus, Phys. Rev. A **83**, 013412 (2011).
[35] X. Xie, K. Doblhoff-Dier, S. Roither, M. S. Schöffler, D. Kartashov, H. Xu, T. Rathje, G. G. Paulus, A. Baltuška, S. Gräfe, and M. Kitzler, Phys. Rev. Lett. **109**, 243001 (2012).
[36] A. M. Sayler, T. Rathje, W. Müller, C. Kürbis, K. Rühle, G. Stibenz, and G. G. Paulus, Opt. Express **19**, 4464 (2011).
[37] L. Zhang, S. Roither, X. Xie, D. Kartashov, M. Schöffler, H. Xu, A. Iwasaki, S. Gräfe, T. Okino, K. Yamanouchi, A. Baltuska, and M. Kitzler, J. Phys. B **45**, 085603 (2012).
[38] X. Xie, S. Roither, M. Schöffler, E. Lötstedt, D. Kartashov, L. Zhang, G. G. Paulus, A. Iwasaki, A. Baltuška, K. Yamanouchi, and M. Kitzler, Phys. Rev. X **4**, 021005 (2014).
[39] X. Xie, E. Lötstedt, S. Roither, M. Schöffler, D. Kartashov, K. Midorikawa, A. Baltuška, K. Yamanouchi, and M. Kitzler, Sci. Rep. **5**, 12877 (2015).
[40] X. M. Tong and C. D. Lin, J. Phys. B **38**, 2593 (2005).
[41] P. Wustelt, M. Möller, M. S. Schöffler, X. Xie, S. Roither, D. Kartashov, A. M. Sayler, A. Baltuska, G. G. Paulus, and M. Kitzler (unpublished).
[42] A. Tong, Y. Zhou, and P. Lu, Opt. Express **23**, 15774 (2015).
[43] M. V. Ammosov, N. Delone, and V. P. Krainov, Sov. Phys. JETP **64**, 1191 (1986).
[44] G. L. Yudin and M. Y. Ivanov, Phys. Rev. A **64**, 013409 (2001).
[45] G. G. Paulus, F. Grasbon, A. Dreischuh, H. Walther, R. Kopold, and W. Becker, Phys. Rev. Lett. **84**, 3791 (2000).
[46] See Supplemental Material at http://link.aps.org/supplemental/10.1103/PhysRevA.93.063421 for animated versions of the CEP-resolved measured ion momentum distributions.
[47] G. Paulus, W. Nicklich, F. Zacher, P. Lambropoulos, and H. Walther, J. Phys. B **29**, L249 (1996).
[48] W. A. Bryan, S. L. Stebbings, J. McKenna, E. M. L. English, M. Suresh, J. Wood, B. Srigengan, I. C. E. Turcu, J. M. Smith, E. J. Divall, C. J. Hooker, A. J. Langley, J. L. Collier, I. D. Williams, and W. R. Newell, Nat. Phys. **2**, 379 (2006).